Retinal axial focusing and multi-layer imaging with a liquid crystal adaptive optics camera

2014 Chinese Phys. B 23 094211

(http://iopscience.iop.org/1674-1056/23/9/094211)

Retinal axial focusing and multi-layer imaging with a liquid crystal adaptive optics camera*

Liu Rui-Xue(刘瑞雪)[a)b)], Zheng Xian-Liang(郑贤良)[a)b)c)], Li Da-Yu(李大禹)[a)], Xia Ming-Liang(夏明亮)[c)], Hu Li-Fa(胡立发)[a)], Cao Zhao-Liang(曹召良)[a)], Mu Quan-Quan(穆全全)[a)], and Xuan Li(宣 丽)[a)†]

[a)] *State Key Lab of Applied Optics, Changchun Institute of Optics, Fine Mechanics and Physics, Chinese Academy of Sciences, Changchun* 130033, *China*
[b)] *University of Chinese Academy of Sciences, Beijing* 100049, *China*
[c)] *Jiangsu Key Laboratory of Medical Optics, Suzhou Institute of Biomedical Engineering and Technology, Chinese Academy of Sciences, Suzhou* 215163, *China*

(Received 9 December 2013; revised manuscript received 10 February 2014; published online 23 July 2014)

With the help of adaptive optics (AO) technology, cellular level imaging of living human retina can be achieved. Aiming to reduce distressing feelings and to avoid potential drug induced diseases, we attempted to image retina with dilated pupil and froze accommodation without drugs. An optimized liquid crystal adaptive optics camera was adopted for retinal imaging. A novel eye stared system was used for stimulating accommodation and fixating imaging area. Illumination sources and imaging camera kept linkage for focusing and imaging different layers. Four subjects with diverse degree of myopia were imaged. Based on the optical properties of the human eye, the eye stared system reduced the defocus to less than the typical ocular depth of focus. In this way, the illumination light can be projected on certain retina layer precisely. Since that the defocus had been compensated by the eye stared system, the adopted 512 × 512 liquid crystal spatial light modulator (LC-SLM) corrector provided the crucial spatial fidelity to fully compensate high-order aberrations. The Strehl ratio of a subject with −8 diopter myopia was improved to 0.78, which was nearly close to diffraction-limited imaging. By finely adjusting the axial displacement of illumination sources and imaging camera, cone photoreceptors, blood vessels and nerve fiber layer were clearly imaged successfully.

Keywords: liquid crystal device, adaptive optics, retinal imaging

PACS: 42.70.Df, 42.68.Wt, 42.66.Ew **DOI:** 10.1088/1674-1056/23/9/094211

1. Introduction

Human retina is a thin, transparent, and multi-layered neural tissue. In section the retina is no more than 0.5 mm thick and has ten distinct layers. Many important eye diseases and systemic diseases manifest themselves in the retina. Imaging the retina allows diseases of the eye proper, as well as complications of hypertension, diabetes and other cardiovascular diseases, to be detected, diagnosed, and managed.[1–4] Fundamentally, image quality of the retina is limited by the wave aberrations intrinsic to the cornea and crystalline lens. With the help of adaptive optics (AO) technology, cellular level imaging of living human retina can be achieved.[5–7]

Since the introduction of the AO for the eye, all facets of the AO have great development, including its illumination source, wavefront sensor, wavefront corrector, and control algorithm. For example, high-power superluminescent diode with low coherence is a good choice as the light source for AO system.[8–10] The effectiveness of the AO system to correct ocular aberrations is typically limited by the performance of the wavefront corrector. Various types of wavefront correctors have been employed. Dreher *et al*. used a 13-segment deformable mirror (DM) to compensate for the astigmatism of the eye[11] Liang *et al*. successfully obtained images of cones photoreceptors with a 37 channel mechanical DM.[5] Microelectromechanical (MEMS) DM, more cost effective and smaller, has been successfully applied to the eye.[12–15] Liquid crystal spatial light modulators (LC-SLMs) are an alternative wavefront corrector technology.[16–22] LC-SLMs induce local path-length changes by altering the refractive index rather than translating mirror segments.[23–27] This reflective device is similar to piston-only segmented DM.[28,29] It has a high spatial resolution (typically 480 × 480, 512 × 512, 600 × 800), operates with low control voltages (∼ 5 V) and has a good repeatability and no hysteresis.[30–36]

Due to the presence of archetypal levels of second-order aberrations, AO retina cameras with any single kind of wavefront corrector have not achieved to yield diffraction-limited imaging across large pupils (≥ 6 mm). To achieve the goal, it is necessary to fully compensate both low- and higher-order aberrations of the eye. Generally, trial lenses or Badal systems are employed to reducing defocus. Even if subjects were meticulously refracted with trial lenses, according to statistical analysis,[37] the peak-to-valley (PV) error for 7.5-mm pupil ranges from 7 to 11 μm depending on the second-order

*Project supported by the National Natural Science Foundation of China (Grant Nos. 60736042, 1174274, and 1174279) and the Plan for Scientific and Technology Development of Suzhou, China (Grant No. ZXS201001).

†Corresponding author. E-mail: xuanli@ciomp.ac.cn

state. Employing Badal systems is another approach to reducing defocus.[38,39] However, they make the main optical path more complex. Meanwhile, cycloplegia drugs are usually used to freeze accommodations of the eyes. In this situation, the crystalline lenses are fixed to focus far point of the eyes, which is beneficial to accurately choose a certain degree trial lens and decrease accommodation errors. Usually, the drugs do not have a serious side effect in clinical use, while uncomfortable feelings were inescapable. For example, Tropicamide, which is superior to others because of shorter half-life, induces stinging and may cause an attack of acute angle-closure glaucoma in rare cases.

Aiming to reduce uncomfortable feelings and avoid potential drug induced diseases, we attempted to image retina with dilated pupil and frozen accommodation without drugs. A simple method to dilate pupil is to decrease the background luminance. Due to sufficient illumination light for wavefront detecting and imaging, the accommodation response always exists. In this case, a structured visual target will be positioned to guide the lens power. Compared with paralyzing eyes, an obvious difference is that the focus error should be considered in accommodation eyes. For the depth-of-focus effects, the image on the retina is not so sharp in fact, while one believe himself/herself watching the target clearly. Thus, if the target is still considered as the image plane, there will be a defocus aberration in optical path, which introduces uneven illumination and decreases the effectiveness of detection and correction.

For reducing focus error in accommodation eyes and improving retinal positioning accuracy, this paper demonstrates a human eye stared system in a novel liquid crystal adaptive optics retinal camera. Based on the ability of the ocular accommodation, the eye stared system reduced the defocus to less than the typical ocular depth of focus. Thus, the LC-SLM corrector provided the crucial spatial fidelity to fully compensate high-order aberrations. By finely adjusting the axial displacement of the visual target, light sources and imaging camera, different layers of the retina were imaged successfully.

2. Experimental setup and method

The schematic diagram of the system is illustrated by Fig. 1. The open-loop AO camera setup has been described previously.[31] The modifications made to the instrument for this article involve the light delivery portion, the visual target and the axial displacement control. Therefore, explanation of the instrument setup will concentrate on describing those parts of the instrument, with a brief review of the wavefront sensing and wavefront compensation components.

2.1. Subjects

Four normal Chinese males, between the ages of 24 and 34, were imaged. They were denoted by S1, S2, S3, and S4 in the order of the degree of myopia in the right eye, which

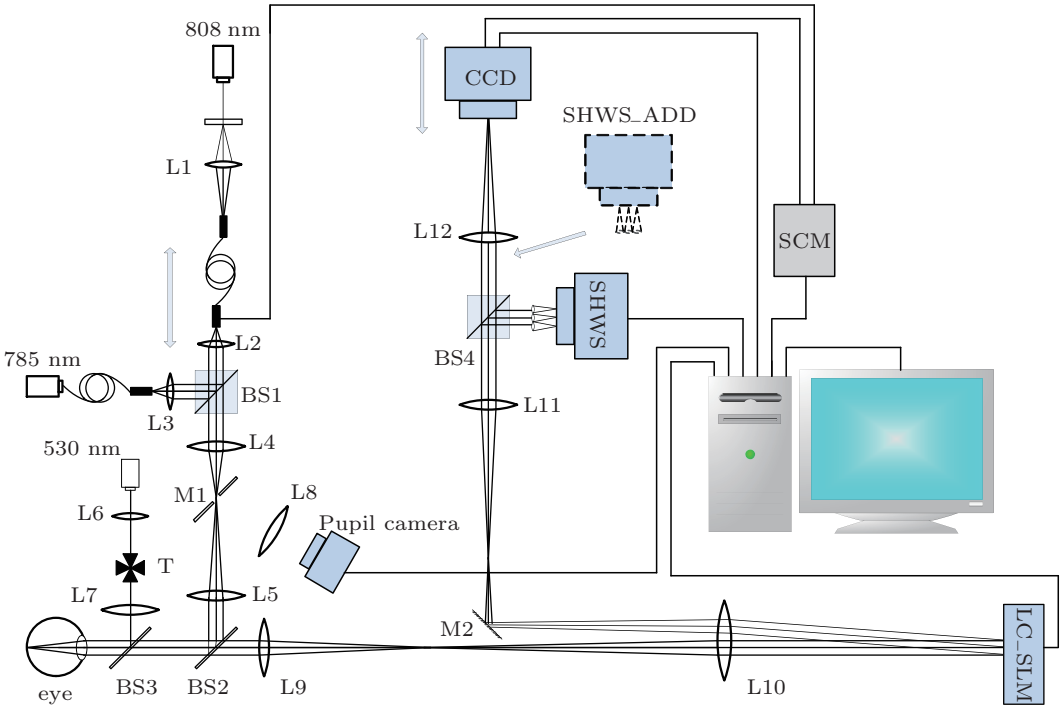

Fig. 1. (color online) Schematic of the AO system. L: lens. M: mirror. BS, beam splitter. T: visual target. Pupil camera: the camera used for aligning the human pupil. CCD: charge-coupled device, the imaging camera. LC-SLM: liquid crystal spatial light modulator. SHWS: Shack–Hartmann wavefront sensor. SHWS_ADD, the added SHWS for sensing residual aberrations. SCM: single-chip microcomputer. Wavelenghth of three light sources are 530 nm, 785 nm, and 808 nm, respectively. The position of the 808 nm light source and the CCD can be moved in the axial direction.

was 0 diopter (D), −2.5 D, −3.5 D, and −8 D, respectively. Trial lenses were used to correct myopia. All subjects gave prior written consent in accordance with the Declaration of Helsinki. In a dark room for 5–15 minutes, pupils of all subjects got wider than 6 mm, which was the size of the designed stop.

2.2. Light delivery

Fitting to the minimal irritation, near-infrared wavelengths are preferred as illumination sources, no matter for sensing and imaging. Thus, pupils without drugs can keep dilating for a long time and a small number of frames will be collected. The wavelengths of the sources should be different but close, in order to separate the lights by dichroic beam splitters (DBS) and reduce chromatic aberration if possible. Therefore, 780 nm and 808 nm are chosen as the sensing and imaging wavelength, respectively.

The 780-nm source is a superluminescent diode (SLD) with a bandwidth of about 20 nm. Light from the SLD focuses on the photoreceptor layer, forming a round spot with a diameter of about 50 μm, which is considered as a "point" for the SHWS to measure aberrations accurately. One degree (about 300 μm) imaging field-of-view (FOV) was lighted by an 808-nm semiconductor laser diode (LD). A rotating scatter plate (thin frosted glass) was used to reduce laser speckle.[30] Each source is coupled into a single mode optical fiber and is collimated by an aspheric lens. The fiber pigtail of the 808-nm LD can move in the direction of optical axis for focusing different retinal layers.

Annular illumination pupils with 0.45 normalized inner radii are used for reducing reflected light from the cornea and improving transverse resolution.[40] Annular illumination pupils are aligned so that they are all conjugate to the entrance pupil of the eye.

During one control loop to 40 ms, one frame is recorded. The pulse time of sensing light and imaging light is 3 ms and 6 ms, respectively, and the CCD exposure time is 5 ms. The irradiance on the retina is 3.5 mW/mm^2, which is approximately 1/20 of the maximum permissible exposure (MPE) according to ANSI.Z136.1-2007.[41]

2.3. Eye stared system and accommodation measurement

The eye stared system contains a telecentric optical path construction and a structured visual target, a Maltese cross. The Maltese cross is illuminated by a beam of parallel light. The back focus of the lens L7 coincides with the entrance pupil of the eye. Thus, the image of the target on the retina can keep a constant size when the target moves, which avoids physiological and psychological changes of different spatial frequency. The focal length of L7 is 100 mm. When the target moves from the anterior focal point to the lens surface, accommodation stimulation gradually changes from 0 D to 10 D. The radius of L7 determines the range of the imaging area of the retina. The location choice is controlled by the eye ball moving. If attempting to image a 10 degree location from the central fovea, the radius is at least 17.3 mm. A lens with a diameter of 40 mm was adopted in the realistic experiment.

The visual target is used for stimulating accommodation and fixating imaging area. All the subjects were told to stare at the target clearly as possible as they can. Owing to that the photoreceptors layer is the layer to receive light signals, the target forms a sharp image on this layer when one stares a target clearly. According to the position of the target, we can know where the photoreceptors layer is. If the illumination source and the imaging camera keep conjugating with the target, we can believe that they just concentrate on the photoreceptors layer.

However, although the target does not form a sharp image on the photoreceptors layer, one believes himself/herself gaze at the target clearly, due to the existence of the ocular depth-of-focus. This phenomenon is named accommodation errors (or focus errors, steady-state errors), which is an intrinsic part of the accommodation control system.[42] Accommodation errors are usually characterized by overaccommodation for distant object and underaccommodation for near object. In this case, if the illumination source and the imaging camera still keep conjugating with the target, they cannot focus on the photoreceptors layer. The accommodation errors of subjects are measured with naked eyes and with refracted eyes by trial lenses, which are shown in Figs. 2(a) and 2(b), respectively. The accommodative stimulus is the power of the target distance away from the eye pupil. The accommodative response is the diopter of the eye when the subjects stared the target clearly, which is calculated by the defocus aberration measured by the SHWS. The differences between the stimulus and the response are the accommodation errors. Theoretically, as long as in the accommodation range, the target can be positioned anywhere. The relevance between the ocular power and the target distance can be continuously established. A phenomenon is that the accommodative response and the stimulus usually are alike at 1 D or so. Put the target at the "equal position", the physical location of the image of the photoreceptors layer can be easily determined. In the experiment, the target was just moved at the 1 D position away from the eye.

The designed illumination light and the reflection light from the retina are both considered as parallel lights at the position of the pupil of the eye. There will be a problem with the 1 D target. As mentioned above, both the target and the

sensing source should be conjugated with the photoreceptor layer, but they are positioned at 1 D and infinite distance, respectively. In this case, the longitudinal chromatic aberration (LCA) of the human eye is introduced to compensate for the displacement. The LCA is fairly consistent between individuals so we can estimate where the correct focus must be.[15] In this case, according to the Cauchy equation,[43] a green LED (530±10 nm, at less than 30 Trolands) was adopted to brighten the target. Thus, the power of the eye lens was approximately 1 D for green target and 0 D for near-infrared illumination light.

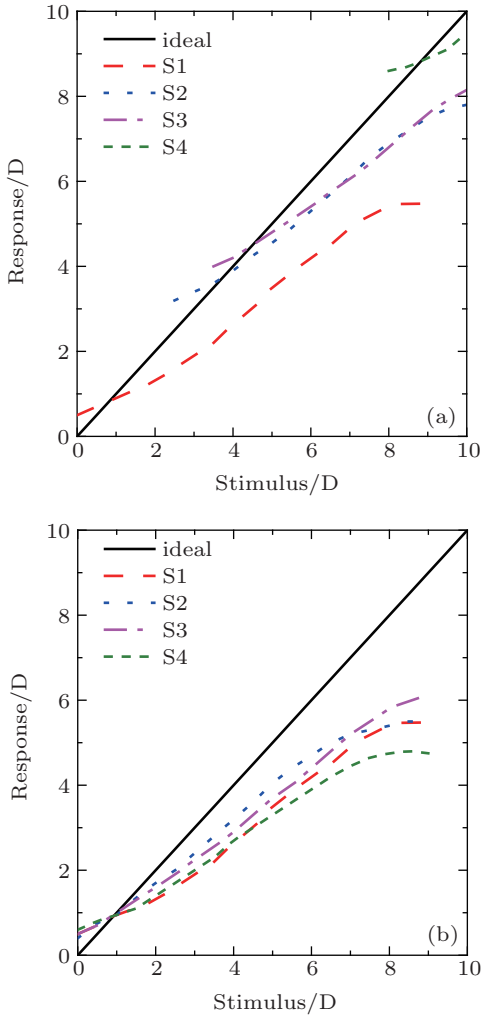

Fig. 2. (color online) Accommodative stimulus/response curve (a) without trial lenses and (b) with trial lenses. The 1:1 solid line represents the ideal accommodative stimulus/response profile. The dashed lines represent realistic accommodative response profile of the four subjects.

2.4. Performance of the AO system

The adopted LC-SLM corrector has an active area of 7.68 mm × 7.68 mm and 512 × 512 pixels. A Shack–Hartmann wavefront sensor (SHWS) with a lenslet array of 0.216 mm × 0.216 mm pitch and 7.315 mm focal length is employed to measure the eye's wavefront. A seven-order Zernike polynomial is fitted to the wavefront slopes.

LC-SLMs change the refractive index to adjust the optical path. LC-SLMs are limited to phase modulation. Extended stroke can be achieved with phase wrapping. Generally, second-order aberrations dominate the total ocular wavefront error. Suppose the spherical wave is supposed to propagate to the LC-SLM. The magnitude on the edge is the largest. The number of modulo-2π N can be expressed as

$$N\lambda = R - (R^2 - L^2)^{1/2}, \tag{1}$$

$$(N-1)\lambda = R - [R^2 - (L-S)^2]^{1/2}, \tag{2}$$

where λ is the imaging wavelength, R is the radius of the spherical wave, L is the radius of the LC-SLM, and S is the projective length of the edge mode on the LC-SLM. For a given LC-SLM, L can be considered as a constant. Based on Eqs. (1) and (2), the relationship between R and S is given by

$$S = L - [-\lambda^2 + L^2 - 2\lambda(R^2 - L^2)^{1/2}]^{1/2}. \tag{3}$$

When $R \in (L, +\infty)$, S is an increasing function of R, which means that larger defocus aberration corresponds to fewer pixels to fitting wavefront at the edge.

The correction performance of the LC-SLM cannot be judged directly, because residual aberrations cannot be measured in the employed open-loop control mode. To solve the problem, an added SHWS is used for sensing the residual aberrations. As showed in Fig. 1, the added SHWS is positioned instead of the imaging lens L12 and the imaging camera. The lenslet of the added SHWS is conjugated with the eye pupil and the LC-SLM. In this way, we can obtain the residual aberrations after AO correction to know the effectiveness of the system with or without the eye stared system.

2.5. Multi-layer imaging

As mentioned above, the image plane of the photoreceptor layer can be determined by the visual target. Aiming to illuminate and image other layers, the imaging source and the camera will be moved a certain distance together from the initial position. Designed axial magnification between the 808-nm imaging source and the camera is about 150×. A single-chip microcomputer (SCM) is employed to control the two displacement motors. For a routine eye model with an 18 mm effective focal length, if the focus plane from the photoreceptor layer to the nerve fiber layer (about 0.3 mm), the displacement of the imaging source and the camera are 0.28 mm and 43.2 mm, respectively.

3. Results and discussion

3.1. Retinal axial focusing accuracy

According to Fig. 2, we know that the accommodative response and the stimulus are commonly alike at 1 D or so, but not exactly at 1 D. There are so many factors that influence the result, including target form and contrast,[44] ocular pupil

diameter,[45] and luminance level.[46] Furthermore, when a target at a fixed distance is viewed with steady fixation, the accommodative response typically shows slight fluctuations.[47]

In our observing conditions, which have been described in the previous chapter, the accommodation accuracy was measured by the added SHWS. The added SHWS measured the defocus aberration, which was the accommodative response. One hundred data of each subject was recorded. Statistical sum, mean value, and standard deviation were calculated using Matlab software (MathWorks, Inc., US). The maximum focus error was the retinal axial focusing accuracy. Figure 3 shows the statistical sum of the accommodative responses of the subjects when the target was placed at the 1 D position. The mean value of the accommodation and its standard deviation is 0.97 D±0.06 D. 95 percent of the data (two times the standard deviation) is distributed from 0.85 D to 1.09 D. The maximum focus error is $0.85 - 1 = -0.15$ D.

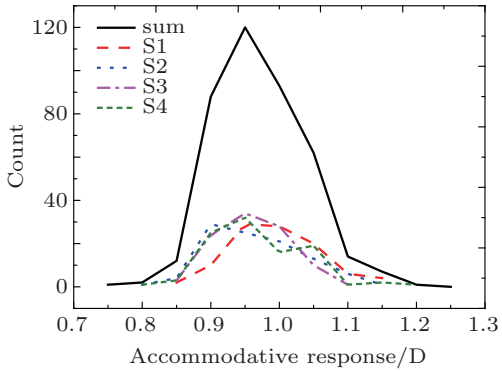

Fig. 3. (color online) Accommodative response distribution curve with a 1 D target. 100 statistical data of each subject were recorded. The black solid line represents the sum of statistical data of all subjects.

The retinal axial focusing accuracy has respect to the focus accuracy of the illumination. If the focus range of the illumination is positioned in the ocular depth-of-focus, it can be considered focusing accurately. For the eye, the depth-of-focus is the range of object distances for which image quality is not significantly degraded, which depends on a variety of optical and neural factors. Typically, the ocular depth of focus is in the range from ±0.25 to ±0.5 D.[48] Thus, the maximum focus error of −0.15 D with the 1 D target is less than the depth of focus and the illumination light can be projected on a certain retina layer precisely.

3.2. AO practical effectiveness with the eye stared system

Figure 4 shows that the PV errors of the defocus caused by the accommodation error and other aberrations. The PV errors and the Zernike coefficients were calculated using Matlab software. The 4th Zernike mode corresponds to defocus and the 3rd and 5th mode are astigmatisms. The PV error of the low-order aberrations can be calculated and is about 2 μm. Miller *et al.* confirmed that for a 6-mm pupil, the LC-SLM with 72×72 pixels can handle 1 D defocus.[49] According to research of spatial properties of ocular aberrations in a large population of 100 normal eyes, about 100×100 segmented piston-only actuators are needed to compensate higher-order ocular aberrations.[6] However, they did not consider the diffractive characteristics of the LC-SLMs. Based the aforementioned research,[28] if the quantified level is larger than 10 to maintain nearly 85% diffraction efficiency and a continuous wavefront profile, the projective length of the edge mode $S = 10 \times (7.68 \div 512)$ mm $= 0.15$ mm. According to Eq. (3), about 222×222 pixels can correct 1 D defocus and at least 300×300 pixels can compensate higher-order ocular aberrations. Hence, for fully compensating higher-order aberrations, the low-order ocular aberrations (defocus and astigmatism) should be below 1 D (4.5 μm PV error with 6 mm pupil) for the 512×512 LC-SLM. As mentioned above, the PV error of the low-order aberrations is about 2 μm, which can meet the requirement.

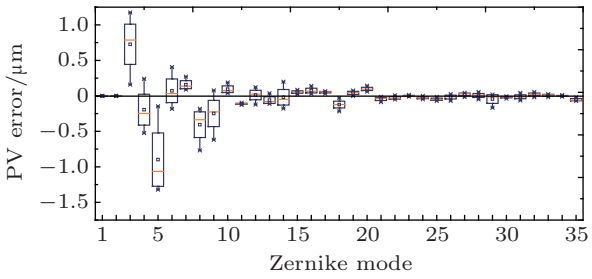

Fig. 4. (color online) PV wavefront errors of top 35 Zernike modes of four subjects.

Figure 5 shows the sensed wavefront for subject S4 with and without the eye stared system. S4 was −8 D myopia and meticulously refracted with trial lenses. Usually, patients with extreme myopia have more complex higher-order aberrations. In the previous AO system, S4 stared a 4 D target directly.[31] Due to the accommodation error, regardless of the fact that S4 refracted with trial lenses, a large defocus (several rings in the wavefront) can be observed in Fig. 5(a). If the LC-SLM was only used to correct both the low- and the complex higher-order aberrations of the eye, the corrector struggles to provide compulsory high spatial fidelity and high dynamic range. The wavefront after AO correction without the new eye stared system is showed in Fig. 5(b). The eye stared system compensates the defocus and the wavefront before AO correction is showed in Fig. 5(c). Due to fully compensating higher-order aberrations, compared with the wavefront without the additional eye stared system, a more smooth wavefront was obtained with the new eye stared system after AO correction, which is showed in Fig. 5(d). The point spread functions (PSFs) of the two AO correction results without and with the eye stared system is

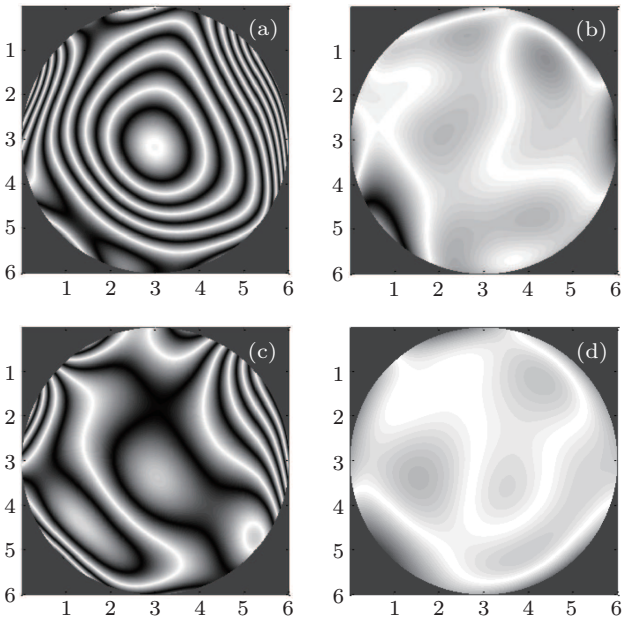

Fig. 5. Wavefront for subject S4, (a) without the eye stared system and before AO compensation, PV = 7.11 μm, RMS = 1.39 μm; (b) without the eye stared system and after AO compensation, PV = 0.96 μm, RMS=0.10 μm; (c) with the eye stared system and before AO compensation, PV = 4.41 μm, RMS = 0.68 μm; (d) with the eye stared system and after AO compensation, PV = 0.45 μm, RMS = 0.06 μm. The coordinates represent the 6 mm human pupil.

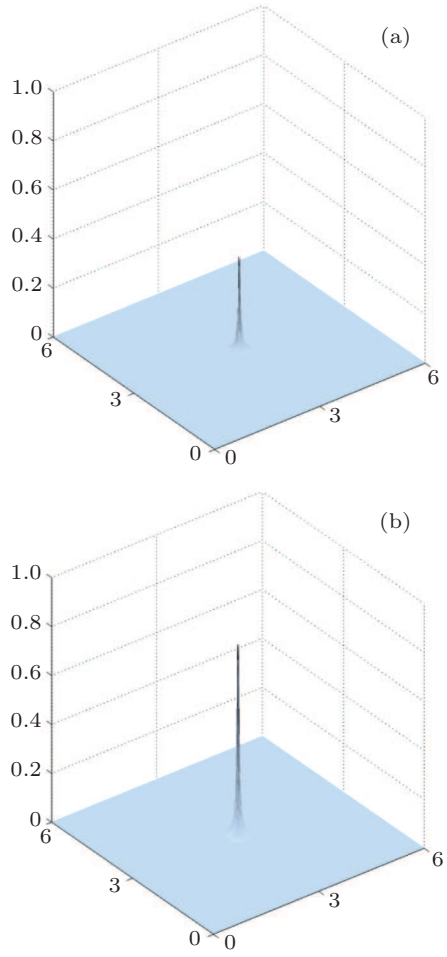

Fig. 6. (color online) (a) Point spread function of Fig. 5(b). The Strehl ratio is 0.37. (b) Point spread function of 5(d). The Strehl ratio is 0.78.

shown in Figs. 6(a) and 6(b), respectively. PSF describes the response of the imaging system to a point source, which was calculated using Matlab software. By the eye stared system to correct the eye's low-order wave aberration for the 6 mm pupil, the PSFs suggest that the present system has created a twice as much increase in the Strehl ratio. The Strehl ratio is improved from 0.38 to 0.78, which is nearly close to diffraction-limited (Strehl ratio = 0.8). Through the above results and analysis, the eye stared system is proved to be benefit for the system to improve the ability of fully compensating aberrations.

3.3. Imaging

Figure 7 shows images of photoreceptors at 2° location away from the central fovea for subject S3. We could not visualize any significant contrast or the microscopic structure of the retina without the AO compensation and without the eye stared system, which is showed as Fig. 7(a). After defocus correction by the eye stared system, some fuzzy spots can be observed in Fig. 7(b). Figure 7(c) is taken with the eye stared system and AO correction. Cone photoreceptors could be resolved clearly in this figure.

Figure 8 shows the computed power spectra of the images shown in Fig. 7 using Matlab software. Power spectrums describe how the power of the images is distributed over different spatial frequencies. The power spectrum of the image obtained with adaptive compensation is shown in Fig. 8(c). It contains power in a ring of spatial frequencies, the signature of the cone mosaic first described in spectra of anatomical sections.[50] This ring is not evident in the power spectrum of the image obtained without compensation. As shown in the Fig. 8(b), despite the fact that the ring cannot be observed, the high-frequency components of the power spectrum of the image are improved after the defocus compensation. The images of cone photoreceptors (Fig. 7) and the power spectra (Fig. 8) indicate that eye stared system can help improve the imaging quality. Even if the cone photoreceptors cannot be resolved without the AO compensation, more details and more high-frequency spatial information can be obtained with the help of the eye stared system.

The eye stared system is proved to be benefit for the system to improve the ability of fully compensating aberrations. The stared system compensates the defocus and the LC-SLM corrects astigmatisms and the complex higher-order aberrations. Although the retinal axial focusing accuracy is less than the ocular depth-of-focus, about 0.15 D focus error should be compensated by the wavefront corrector. Actually, astigmatisms can also be compensated by trial lenses. If the low-order aberrations (defocus and astigmatisms) can be more accurately compensated by the eye stared system and trial lenses, the

wavefront corrector can correct high-order aberrations much more fully and provide higher imaging resolution. Besides, a higher accuracy wavefront detector and more effective control algorithms are beneficial for improving the correction accuracy and the imaging resolution. Imperfect adaptive compensation may be further improved by post-processing techniques such as inverse filtering and image registration.

In this experiment, for fitting to the minimal irritation, near-infrared wavelengths were selected as illumination sources. Human eye is insensitive to near-infrared light. For further improving the imaging resolution, shorter wavelength source can be employed for illuminating the retina in a future experiment. AO's role in a retinal camera is to compensate high-order aberrations and to realize diffraction-limited imaging through the highest possible numerical aperture in the eye. Theoretically, a larger human pupil introduces higher imaging resolution. In this paper, being to reduce uncomfortable feelings and avoid potential drug induced diseases, we attempted to image retina with dilated pupil and frozen accommodation without drugs but in a dark room. For the healthy young subjects, pupils can get wider than 6 mm. However, for the aging, illness or injured eyes, pupils possibly cannot get wider than the size of the designed stop of the system. In such circumstances, mydriatic need to be employed to take advantage of the reduced diffraction. The axial resolution grows as the square of the pupil diameter, which is critical in optical sectioning of the retina in depth. If 555 nm illumination and an 8 mm pupil were used, a two-fold increase will be realized in imaging resolution and theoretically increase the axial resolution of by a factor of 4.

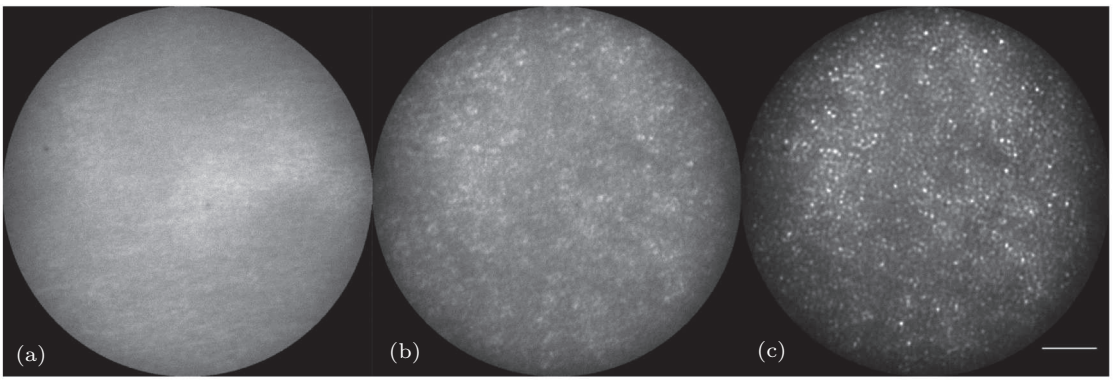

Fig. 7. Photoreceptor images (a) without eye stared system and before the AO compensation, (b) with eye stared system and before the AO compensation and (c) with eye stared system and after the AO compensation for the subject S3, respectively. The white bar represents 50 μm.

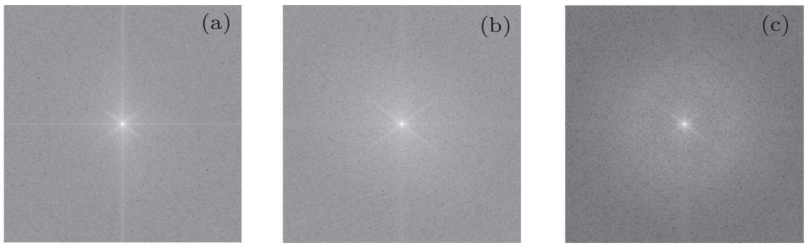

Fig. 8. Computed power spectra of the photoreceptor images shown by Figs. 7(a)–7(c), respectively.

Figure 9 shows different tissues images for subjects S1 and S2 at the same location and different axial positions. Photoreceptors, blood vessels and nerve fiber bundles are observed gradually with the axial moving. While in these images, compared with images of cone photoreceptors, some details of the blood vessels and nerve fiber bundles are not so clear. Cone photoreceptors have high reflectance and contrast. However, other tissues in the retina scatter very little light and have less contrast. According to different optical properties of different tissues, manipulation of the imaging wavelength and polarization might be used to improve contrast. To achieve an image with sufficient contrast, an important method is to transfer as much of available contrast from the object to the image. This is realized by making the modulation transfer function (MTF) as high as possible. For example, a simplified system with less optical elements can effectively decrease energy loss and increase MTF.[20] Besides the retinal camera, the eye stared system can also be integrated into adaptive optics scanning laser ophthalmoscope (AO-SLO) and adaptive optics optical coherence tomography (AO-OCT). Confocal imaging in SLO or co-

herencegated detection in OCT can increase the lateral and axial MTF. In this way, SLO or OCT provides higher imaging contrast and the eye stared system helps wavefront corrector to fully compensate both low- and higher-order aberrations.

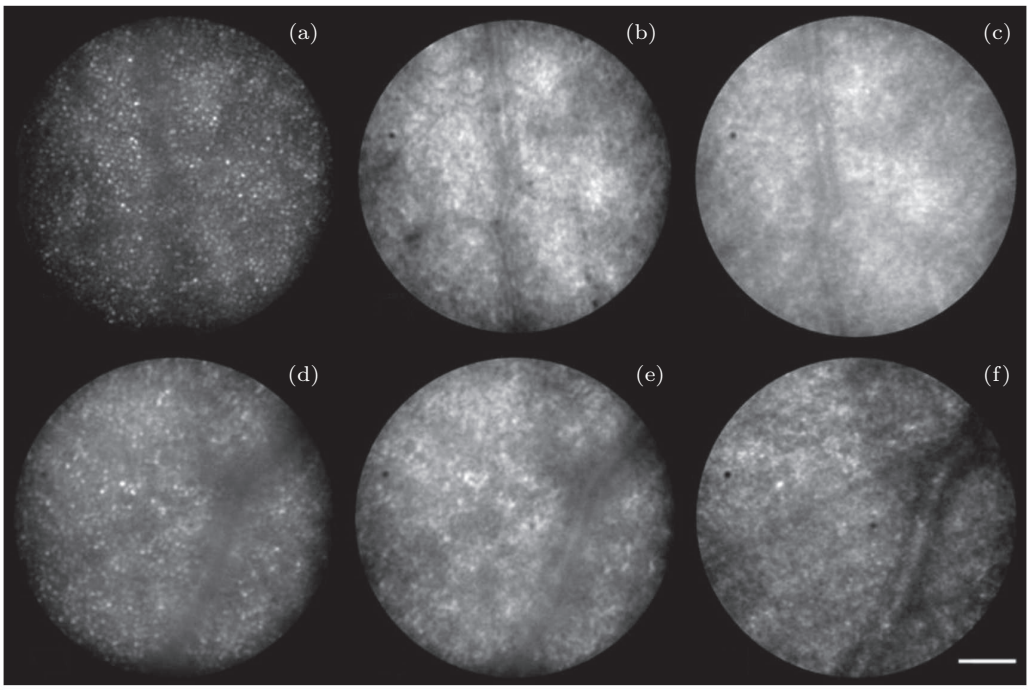

Fig. 9. Multi-layer retinal images after the AO compensation for the subjects S1 and S2, respectively. (a), (d) Cone photoreceptors, (b), (e) blood vessels, and (c), (f) nerve fiber layer are imaged gradually with the axial moving. The white bar represents 50 μm.

4. Conclusion

In summary, a liquid crystal AO ophthalmoscope was presented for accommodation eyes. The optical design reduced the accommodation error to below the ocular depth-of-focus. Thus, the illumination light can be projected on certain retina layer precisely and the performance of LC corrector became more effective for higher-order aberrations. Various retinal tissues had been imaged successfully. The eye stared system can be applied for other kind correctors, which also face the barrier between high spatial precision and high dynamic range. Similarly, the method for accommodation eyes can transplant into other imaging approaches, such as SLO or OCT. We hope that this study promotes further understanding about mechanism and morphology of human vision and diseases associated with human retina.

References

[1] Kitaguchi Y, Fujikado T, Bessho K, Sakaguchi H, Gomi F, Yamaguchi T, Nakazawa N, Mihashi T, and Tano Y 2008 *Ophthalmology* **115** 1771
[2] Zhong Z, Petrig B L, Qi X and Burns S A 2008 *Opt. Express* **16** 12746
[3] Martin J A and Roorda A 2005 *Ophthalmology* **112** 2219
[4] Duncan J L, Talcott K E, Ratnam K, Sundquist S M, Lucero A S, Day S, Zhang Y and Roorda A 2011 *Invest. Ophthalmol. Vis. Sci.* **52** 1557
[5] Liang J, Williams D R and Miller D T 1997 *J. Opt. Soc. Am.* **14** 2884
[6] Doble N, Miller D T, Yoon G and Williams D R 2007 *Appl. Opt.* **46** 4501
[7] Roorda A and Williams D R 1999 *Nature* **397** 520
[8] Zang Z G, Minato T, Navaretti P, Hinokuma Y, Duelk M, Velez C and Hamamoto K 2010 *IEEE Photonics Technology Letters* **22** 721
[9] Zang Z G, Mukai K, Navaretti P, Duelk M, Velez C and Hamamoto K 2012 *Appl. Phys. Lett.* **100** 031108
[10] Zang Z G, Mukai K, Navaretti P, Duelk M, Velez C and Hamamoto K 2011 *IEEE Trans. Electron.* **E94c** 862
[11] Dreher A W, Bille J F and Weinreb R N 1989 *Appl. Opt.* **28** 804
[12] Doble N, Yoon G, Chen L, Bierden P, Singer B, Olivier S and Williams D R 2002 *Opt. Lett.* **27** 1537
[13] Zhang Y, Poonja S and Roorda A 2006 *Opt. Lett.* **31** 1268
[14] Hammer D X, Ferguson R D, Bigelow C E, Iftimia N V, Ustun T E and Burns S A 2006 *Opt. Express* **14** 3354
[15] Grieve K, Tiruveedhula P, Zhang Y and Roorda A 2006 *Opt. Express* **14** 12230
[16] Thibos L N and Bradley A 1997 *Optom. Vis. Sci.* **74** 581
[17] Vargas-Martin F, Prieto P M and Artal P 1998 *J. Opt. Soc. Am. A* **15** 2552
[18] Mu Q, Cao Z, Li D, Hu L and Xuan L 2007 *Opt. Express* **15** 1946
[19] Liu C, Mu Q Q, Hu L F, Cao Z L and Xuan L 2010 *Chin. Phys. B* **19** 064214
[20] Liu R, Qi Y, Zheng X, Xia M and Xuan L 2013 *Photon. Res.* **1** 124
[21] Peng Z, Liu Y, Yao L, Cao Z, Mu Q, Hu L, Lu X, Xuan L and Zhang Z 2011 *Chin. Phys. Lett.* **28** 094207
[22] Dai Q, Li Y, Wu R N, Geng Y, Quan W, Li Y Q, Peng Z H and Yao L S 2013 *Acta Phys. Sin.* **62** 044219 (in Chinese)
[23] Zou Z F, Yao L S, Tang X Z, Ji X J and Xuan L 2008 *Chin. Phys. Lett.* **25** 2524
[24] Liu Y J, Sun W M, Liu X Q, Yao L S, Lu X H and Xuan L 2012 *Acta Phys. Sin.* **61** 114211 (in Chinese)
[25] Tang X Z, Peng Z H, Liu Y G, Lu X H and Xuan L 2010 *Acta Phys. Sin.* **59** 6261 (in Chinese)
[26] Tang X Z, Lu X H, Peng Z H, Liu Y G and Xuan L 2010 *Acta Phys. Sin.* **59** 4001 (in Chinese)

[27] Tian Y, Pan X, Wang C S, Zhang X Q and Zeng Y 2009 *Acta Phys. Sin.* **58** 6979 (in Chinese)
[28] Cao Z L, Mu Q Q, Hu L F, Liu Y G and Xuan L 2007 *Chin. Phys.* **16** 1665
[29] Lu R B, Xu K S, Zhang S Y, Gu X, Xing Z J, Deng H H, Gu J H, Xiao Z D and Lu Z H 1999 *Chin. Phys.* **8** 670
[30] Li C, Xia M, Li D, Mu Q and Xuan L 2010 *J. Biomed. Opt.* **15** 046009
[31] Kong N, Li C, Xia M, Li D, Qi Y and Xuan L 2012 *J. Biomed. Opt.* **17** 026001
[32] Jiang B G, Cao Z L, Mu Q Q, Hu L F, Li C and Xuan L 2008 *Chin. Phys. B* **17** 4529
[33] Liu R, Li D, Xia M, Kong N, Qi Y, Zheng X and Xuan L 2011 2*nd International Symposium on Bioelectronics and Bioinformatics,* November 3–5, 2011 Suzhou, China, p. 135
[34] Takeno K and Shirai T 2012 *Opt. Commun.* **285** 2967
[35] Liu X A, Zhang J A, Wu L Y and Gan Y 2011 *Chin. Phys. B* **20** 024211
[36] Ma J, Zheng Z G, Liu Y G and Xuan L 2011 *Chin. Phys. B* **20** 024212
[37] Thibos L N, Hong X, Bradley A and Cheng X 2002 *J. Opt. Soc. Am. A* **19** 2329
[38] Sawides L, Gambra E, Pascual D, Dorronsoro C and Marcos S 2010 *J. Vis.* **10** 19
[39] Merino D, Dainty C, Bradu A and Podoleanu A G 2006 *Opt. Express* **14** 3345
[40] Sulai Y N and Dubra A 2012 *Biomed. Opt. Express* **3** 1647
[41] Institute A N S 2007 American National Standard for the Safe Use of Lasers (Orlando, FL: Laser Institute of America)
[42] Wang B and Ciuffreda K J 2006 *Surv. Ophthalmol.* **51** 75
[43] Atchison D A and Smith G 2005 *J. Opt. Soc. Am. A* **22** 29
[44] Ciuffreda K J 1991 *Optom. Vis. Sci.* **68** 243
[45] Hennessy R T, Iida T, Shina K and Leibowitz H W 1976 *Vision Res.* **16** 587
[46] Johnson C A 1976 *J. Opt. Soc. Am.* **66** 138
[47] Klein S A 1998 *J. Opt. Soc. Am. A* **15** 2580
[48] Goss D A and Grosvenor T 1996 *J. Am. Optom. Assoc.* **67** 619
[49] Miller D, Thibos L and Hong X 2005 *Opt. Express* **13** 275
[50] Yellott J I 1982 *Vision Res.* **22** 1205